Chapter 11
Heterogeneous Fiber-Particle Composite Subjected to Principal Stress Rotation

Benny Suryanto, Kohei Nagai, and Koichi Maekawa

Abstract Test results of 20 Engineered Cementitious Composite (ECC) plates under 4-point bending are reported. 13 plates were pre-cracked to allow rotation of the principal stress directions, in order to permit the study of shear and tensile stress transfer at multiple cracks. Coarse aggregates were investigated as a possible means to improve shear-transfer. When subjected to principal stress rotation, ECC exhibited a nearly orthogonal crack pattern, indicating little contribution from the shear transfer mechanism. A reduction in flexural capacity was observed, depending on the relative angles of principal tensile stress applied. When coarse aggregate was added to ECC, significant reductions in flexural capacity and flexural ductility were observed. In a situation when principal stress direction rotated, however, the test results show that coarse aggregate in the amount of 15% of the maximum packing density of the aggregate used was effective to control the orientation of secondary cracks in cracked ECC and to maintain a comparable level of flexural capacity irrespective of the reorientation angle of principal stress field and the angle of pre-existing cracks.

11.1 Introduction

Nowadays it is not uncommon to add fibers to improve the properties of concrete in tension. Fibers are expected to reduce the brittleness of concrete and to maintain its integrity after cracking. Depending on the behavior of fiber-reinforced concrete under direct tension and bending tests, Naaman and Reinhardt proposed four

B. Suryanto (✉) • K. Nagai • K. Maekawa
Department of Civil Engineering, The University of Tokyo, 7-3-1 Hongo, Bunkyo-ku, Tokyo 113-8656, Japan
e-mail: benny@concrete.t.u-tokyo.ac.jp; nagai@concrete.t.u-tokyo.ac.jp; maekawa@concrete.t.u-tokyo.ac.jp

M.N. Fardis (ed.), *Innovative Materials and Techniques in Concrete Construction: ACES Workshop*, DOI 10.1007/978-94-007-1997-2_11,

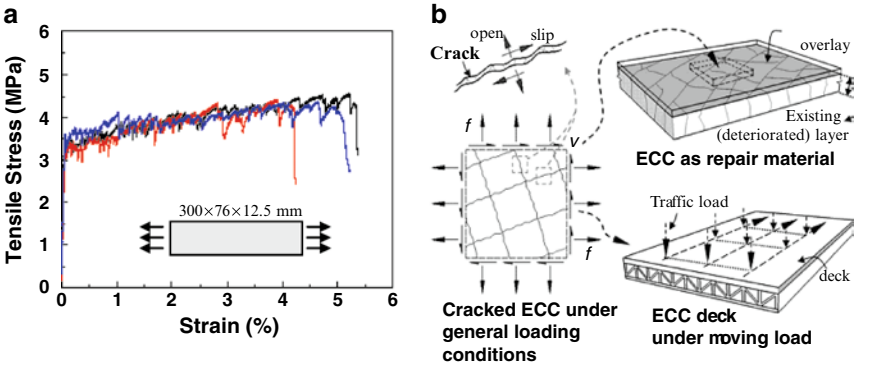

Fig. 11.1 (**a**) ECC with 2% PVA fibers in tension (Li 2003), and (**b**) Illustration of cracked ECC subjected to general loading conditions, allowing not only tensile stress, but also shear stress developed across cracks (Suryanto et al. 2010)

categories: namely, deflection-softening, deflection-hardening, strain-softening, and the outmost remarkable strain-hardening response (Naaman and Reinhardt 1996).

To achieve strain-hardening response in a cement-based composite, (Li and Wu 1992; Li et al. 2001) demonstrated its possibility with a moderate amount of short random polymeric fibers only, a material later known as the Engineered Cementitious Composite (ECC). The strain-hardening response is attributed to the formation of multiple cracks. To achieve this remarkable tensile response, an ECC mixture typically contains fine-graded materials such as cement, fine sand, fly ash, and PVA fibers in a volume ratio of 2% (Li et al. 2001). Example applications of ECC include thin overlays (Kunieda and Rokugo 2006), coupling beams for high-rise buildings (Kunieda and Rokugo 2006), and bridge decks (Kunieda and Rokugo 2006; Li et al. 2005).

In using ECC for general applications, investigation of its post-cracking behavior when subjected to general loading conditions is necessary. Under service loading, cracked ECC may undergo complex behaviors, involving opening, closing, and slip of pre-existing cracks and formation of new cracks. While many investigations have been devoted to investigate the behaviour of ECC relating to the crack-opening (Li 2003), little has been made to investigate the behaviour relating to crack-shear transfer and slip. Crack-shear slip can occur, for example, at the diagonal cracks in shear-critical beams, at the cracks in a bridge deck due to traveling-wheel load, or in an overlay material that has cracked and is under the influence of surrounding damaged parts (Fig. 11.1). In such cases, the rotation of the principal stress fields in the ECC is usually apparent and may proceed to a greater extent. The rotation of stress fields implies that not only tensile stress, but also shear stress develops across cracks. Due to the absence of coarse aggregate, however, it is of concern that cracked ECC may exhibit low interface shear resistance, especially when the crack surface is under repeated shear slip.

To investigate this issue, the authors recently performed bidirectional multiple cracking tests on eight pre-cracked ECC plates (Suryanto et al. 2010). To initiate shear stress at cracks, the test considered two constitutive principal stress directions. The ability of the ECC to transmit tensile and stresses across cracks is evaluated from the remaining flexural capacity, after being pre-cracked, and the final cracking

pattern. The test showed that the flexural capacity of the plates, where the cracks opened and slipped simultaneously, was about 30% (at worst) less than the plates whose cracks were in the opening-mode only. A nearly orthogonal crack pattern was observed irrespective to the difference between the two principal stress directions applied. This suggests that cracked ECC is an orthotropic material, and hence orthogonal cracks resulted. Results of the tests are described in detail in (Suryanto 2009) and are briefly summarized in the following sections.

In response to this finding, this contribution explores the possibility of adding coarse aggregate – referred to as particles in this paper – in ECC with the aim of improving its crack-shear transfer property. Coarse aggregates are recognized as a cheap and potentially available material for use in the fabrication of such a cement-based composite. The scope of this contribution is to come up with a possible mixture proportioning of ECC with coarse aggregate, to check its feasibility, and to investigate the influence of coarse aggregate to the properties of ECC. A more detailed report on the results of a larger series of ongoing investigations on the merit of coarse aggregate in ECC will be given elsewhere. Considering the practical applicability, the current investigation is limited to ECC reinforced with PVA fibers 2% by volume.

11.2 Experimental Program

The experimental program involved the testing of 20 ECC plates produced in three batches. In each batch, there were two types of plate, namely control plates and main plates [see Fig. 11.2a]. The control plates had dimensions of $400 \times 250 \times 20$ mm, whereas the main plates had dimensions of $550 \times 420 \times 20$ mm. The control plates were directly tested in 4-point bending so as to obtain the flexural capacity of the undamaged state. For the main plates, flexural cracks were induced prior to testing. The plates were then sawn with certain orientations to facilitate reorientation of the stress fields and were finally retested in bending to failure. An overview of the experimental program is given in Table 11.1.

11.2.1 Testing Procedure

The overall testing procedure is shown in Fig. 11.2c. To facilitate reorientation of the stress fields, the course of the testing was divided into two testing stages: preloading (stage I) and final loading (stage II). The preloading stage (stage I) was the damage initialization stage and was applied only to the main plates. At this loading stage, the inclination of the principal stress direction was altered by cutting a larger, preloaded plate. This testing technique was inspired by those previously implemented by (Maekawa 1983) and (Van Mier 1985). The damage level was set at 40% of the average ultimate tensile strain of the control plates. The main variable was the orientation of pre-cracks at the plate soffit as listed in Table 11.1. For this purpose, the plate was cut based on the layout given in Fig. 11.2b, with five different orientations: 0°, 20°, 45°, 70°, and 90°.

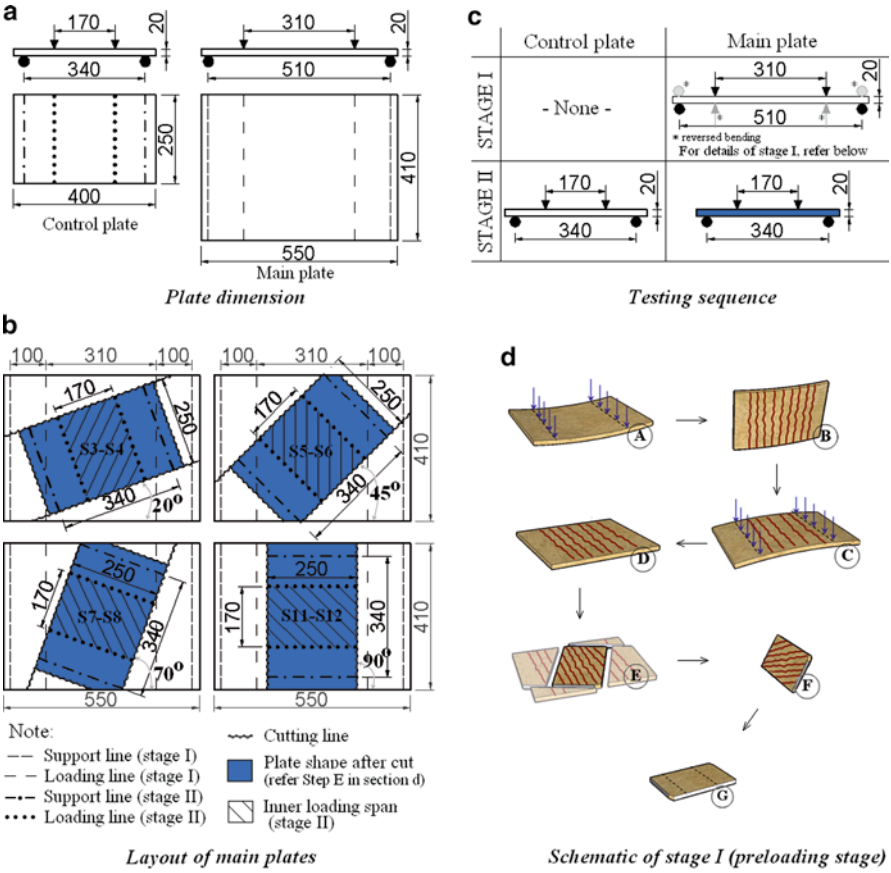

Fig. 11.2 Details of the plates and the testing procedure (Suryanto et al. 2010): (**a**) plate dimension, (**b**) layout of main plates, (**c**) testing procedure, and (**d**) schematic of stage I (preloading stage)

Table 11.1 Overview of test specimen

	Dimension			Initial damage		
ID	W (mm)	L (mm)	H (mm)	Orientation[a](°)	Level (%ε_{tPmax})	Plate type
0C1,2	250	400	20	–	–	Control
0CR						
1C1,2; 2C1,2						
1M0; 2M0	420	550	20	0	40	Main
0M20; 1M20; 2M20				20	40	
0M45; 1M45; 2M45				45	40	
0M70; 1M70; 2M70				70	40	
1M90; 2M90				90	40	

[a] Measured from the plane parallel to the width of the plate after cut 0-, 1-, and 2- implies Group 0, Group 1, and Group 2 plates, respectively

Table 11.2 Mix proportion of ECC and properties of PVA fibers (JSCE 2007)

W/(C+FA) (%)	Water (kg/m^3)	S/(C+FA) (%)	PVA Fibers (% by volume)	Fiber dia. (mm)	Fiber length (mm)	Fiber tensile strength (MPa)
42.2	350	70	2.0	0.04	12	1,600

Table 11.3 Sieve analysis of the coarse aggregate

Sieve size (mm)	Cumulative passing (%)
19	100
13.2	95
4.75	5.7

The complete procedure for the preloading stage is illustrated by the letters A to F in Fig. 11.2d. A step-by-step description of the procedure is as follows:

Step A: The plate was first loaded in a 4-point bending test with a span of 510 mm and an inner span of 310 mm. As loading proceeded, multiple flexural cracks gradually formed at the plate soffit and propagated upwards.

Step B: After reaching the target-damage level, the plate was unloaded and flipped.

Steps C-D: Reversed loading was applied to flatten the plate. As a result of this reversed loading, a few cracks were also observed at the top plate surface. These cracks might slightly reduce the initial stiffness of the plate during the final loading stage.

Step E: The plate was cut so as to align the cracks into the predefined orientation given in Table 11.1 and resize the plate to match the control plate. It was easy to make the cuts while preserving the pre-existing cracks undisturbed.

Step F: At the end of the preloading stage, the plate was flipped again, making it ready for the final loading stage (Step G).

The final loading stage (stage II) was the conventional 4-point bending test and was applied to both control and main plates.

11.2.2 Material Selection and Plate Fabrication

A pre-mixed ECC material (JSCE 2007), of which the mix proportion is listed in Table 11.2, was used. It contained PVA fibers in the volume of 2%. This premix ECC was packed in 25 kg paper bags, and sent to Concrete Laboratory, University of Tokyo, for fabrication of the test plates.

The coarse aggregate was a crushed type available in the market. Its gradation is shown in Table 11.3. Considering the thickness of the test plates, the aggregate size larger than 9.5 mm was omitted. Prior to casting, the aggregate was washed properly and made in the saturated surface dry (SSD) condition. The amount of aggregate included in the Group 1 and 2 was about 30% and 15% of γ_{max}, respectively, where

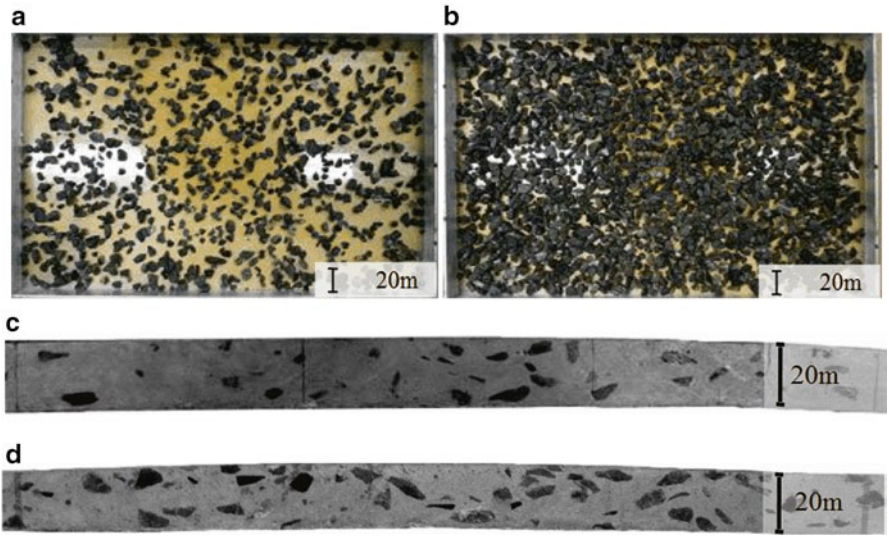

Fig. 11.3 Illustration of the aggregate used in Group 1 and 2 plates: (**a**), (**b**) in 9-mm depth, (**c**) and (**d**) in a sliced section

γ_{max} is the maximum packing density of the aggregate used (about 63%). These two aggregate amounts were decided based on the distribution of the aggregate and the workability when mixed with the ECC paste. Note that the aggregate distribution is important to ensure the presence of aggregate at any potential crack interface, whilst the workability is related to the ease of production. The aggregate used in the Group 2 plates had a minor impact on the workability, while the relatively large amount used for Group 1 had a significant effect. Relatively large addition of aggregate in Group 1 plates was intentionally made for the purpose of investigating the improvement of crack-shear transfer.

Mixing of the ECC was in all cases done as specified in Reference 9 for about 10 min. The air content and slump flow was then measured to ensure the property of the ECC matrix after hardening. The slump flow and air content was 490 mm and 9% for plates in the first batch, 510 mm and 15% for the second batch, and 515 mm and 7% for the third batch. After this measurement, coarse aggregate was added slowly to the ECC slurry in the third bath. They were then remixed for about 2 min.

After mixing, the ECC slurry was poured at once to the middle of each framework, made of plywood with aluminum frames. The slurry was then shredded in a radial pattern, rodded, finished with a steel trowel and finally covered with a plastic sheet. After 2 days, the plates were demolded and air-cured under 60% relative humidity and 20°C until the test date (started from the 28th day after casting). The average compressive strength and modulus elasticity were 33 MPa and 15 GPa, and 39 MPa and 20 GPa respectively, for ECC in the first and third batch, respectively. No measurements were made for ECC in the second batch.

The aggregate included in a 9-mm depth framework is shown in Figs. 11.3a and b. It should be noted that this is a 2D illustration; the distribution in a 3D space was

much sparser. To better illustrate the actual distribution, shown in Figs. 11.3c and d are the aggregate distributions at cut sections of two representative plates. Since the aggregate amount is much less than that used in ordinary concrete, the aggregates appeared to be suspended well in the ECC matrix.

11.3 Macroscopic Response of the Tested Plates

The first part of Sect. 11.3 describes the results of control plates where the influence of coarse aggregate is evaluated in bending under a fixed stress direction. The second part describes the performance of cracked ECC under the rotation of stress fields, which the cracks have to sustain shear and tensile stress actions.

11.3.1 Control Plates (C-Series)

The load-midspan displacement response of all control plates is presented in Fig. 11.4. All control plates exhibited ductile, deflection hardening response. This ductile response attributed to the formation of multiple cracks and the opening of pre-existing cracks. This condition continued until the weakest few cracks were unable to bear the applied tensile stress. Hence, one major localized crack formed across the plate soffit. This was the moment when the plate reached the maximum load.

Although the control plates were made of the same ECC mixture, variation of the first cracking load was observed. This may be attributed to the quality of the ECC matrix caused by the variation of air content for each casting batch. Group 0 control plates (0C1,2) cracked at a load of about 1.6 kN, while Group 1 and Group 2 plates

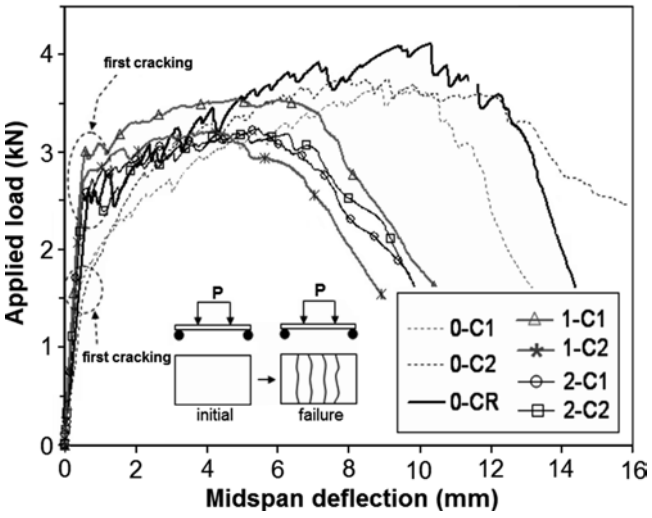

Fig. 11.4 Measured responses of control plates

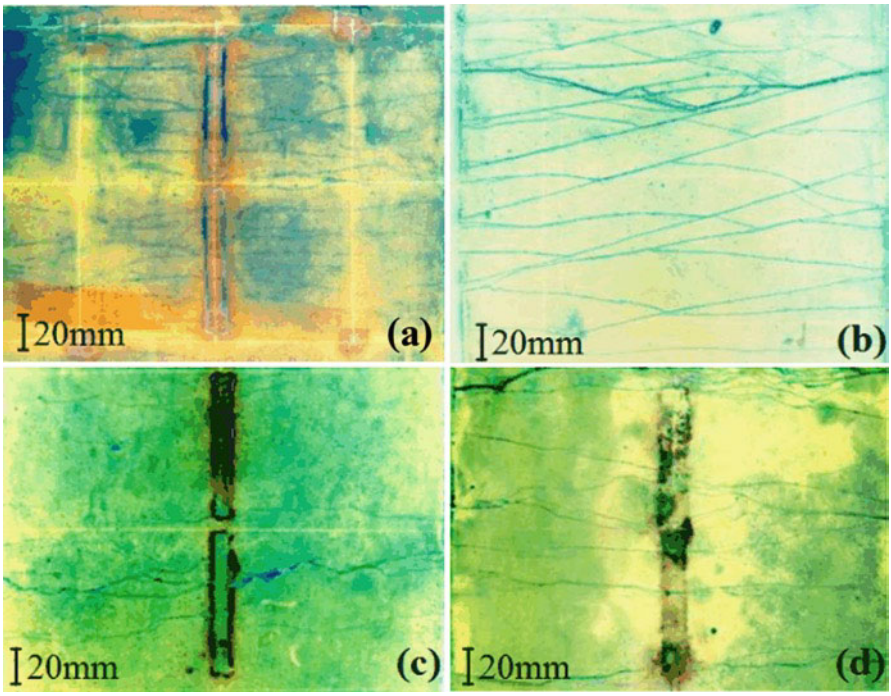

Fig. 11.5 Typical crack pattern after failure: (**a**) Plate 0 C1 (no aggregate); (**b**) Plate 0CR (no aggregate); (**c**) Plate 1 C1 (20%γ_{max}); and (**d**) Plate 2 C1 (10%γ_{max})

[Plates 0CR(no aggregate), 1C1,2, and 2C1,2] were in the range 2.6–2.9 kN. The largest first cracking load was shown by the Group 1 plates with the aggregate addition of 30% γ_{max}. This perhaps indicates the hindrance of aggregate in developing a full-length crack across the plate width.

The post-cracking response of Plates 1C1,2 and 2C1,2 (with aggregate) showed a much flatter response than Plate 0CR (no aggregate). From the response presented in Fig. 11.4 it can be observed that the addition of aggregate decreases the ratio between flexural capacity and cracking load. Flexural capacities of Plates 1C1,2 and 2C1,2 were only about 20% higher than their corresponding cracking load and 20% less than that of Plate 0CR. Moreover, significant reductions in flexural ductility were observed. The average flexural ductility of Plates 1C1,2 and 2C1,2 was about 5.5 mm, half of that of Plate 0CR. The same trend can be seen for the tensile strain measured at the plate soffit at the maximum load. The average strain value was 1.2%, 1.1%, and 0.5% for the first, second, and third batch plates, respectively. These strain values were then used as reference values for determining the initial strain of the main plates. The flexural performance degradations may be attributed to the combination of several factors, including fewer numbers of fiber bridging and increase of the ECC matrix toughness.

Figure 11.5 shows the crack pattern of all control plates over the constant moment span (170 mm). It appears that the higher the aggregate content, the less was the crack

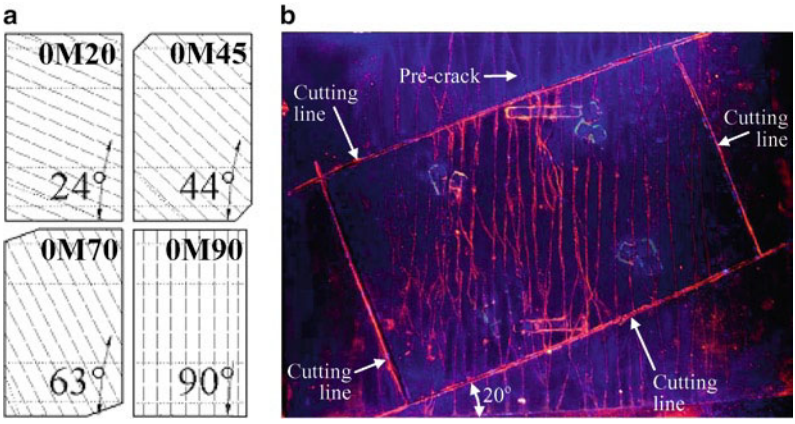

Fig. 11.6 (**a**) Schematic of pre-crack pattern of Group 0 plates, and (**b**) Crack pattern at the soffit of Plate 0 M20 after being pre-cracked and cut

number and the crack width. The crack numbers decreased from about nine cracks in Group 0 [Fig. 11.4b] to six cracks in Group 2 [Fig. 11.4d] and three cracks in Group 1 [Fig. 11.4c] plates. Several microcracks were observed in Group 1 plates.

In general, it appears that the addition of coarse aggregate is accompanied by a decrease in flexural properties including flexural capacity, flexural ductility, and less crack numbers. Perhaps this poor performance explains why coarse aggregate is always omitted in the design of ECC.

11.3.2 Main Plates (M-Series)

The preloading stage resulted in well-established, uniform multiple cracks over the soffit of the main plates. Figure 11.6 illustrates the schematic of the crack pattern for the Group 0 plates prior to the final test. The pre-cracks at the constant moment span prior to the final loading stage were in the range of 10–15 cracks. For Group 1 and 2 plates, no direct observation was made. Judging from the final crack pattern after failure, which will be shown later on in this paper, there were 5–7 cracks prior to the final loading stage.

The load-midspan displacement of Group 0 main plates are compared in Fig. 11.7. Plotted also in the figure are the results of pre-cracked plates that were subjected to higher initial damage level (70% ε_{tu}). Overall, the results indicate that the presence of pre-cracks alters the flexural capacity and initial stiffness of the plates. Notable reductions in flexural capacity were observed in both Plates 0M45 and 0M70. The initial stiffness rises with increasing initial crack orientation up to 90°, indicating the increase contribution of the uncracked ECC between the cracks.

The crack pattern of Group 0 plates are shown in Fig. 11.8. Three typical cracking patterns are observed. First, the cracks appeared in a bi-directional pattern.

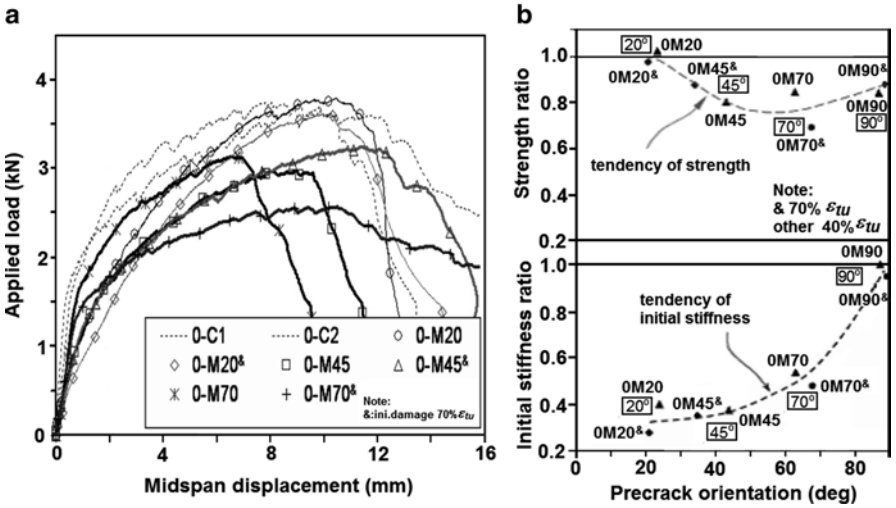

Fig. 11.7 (**a**) Load-midspan deflection of Group 0 plates with no coarse aggregate, and (**b**) Normalized flexural capacity and stiffness of the plates

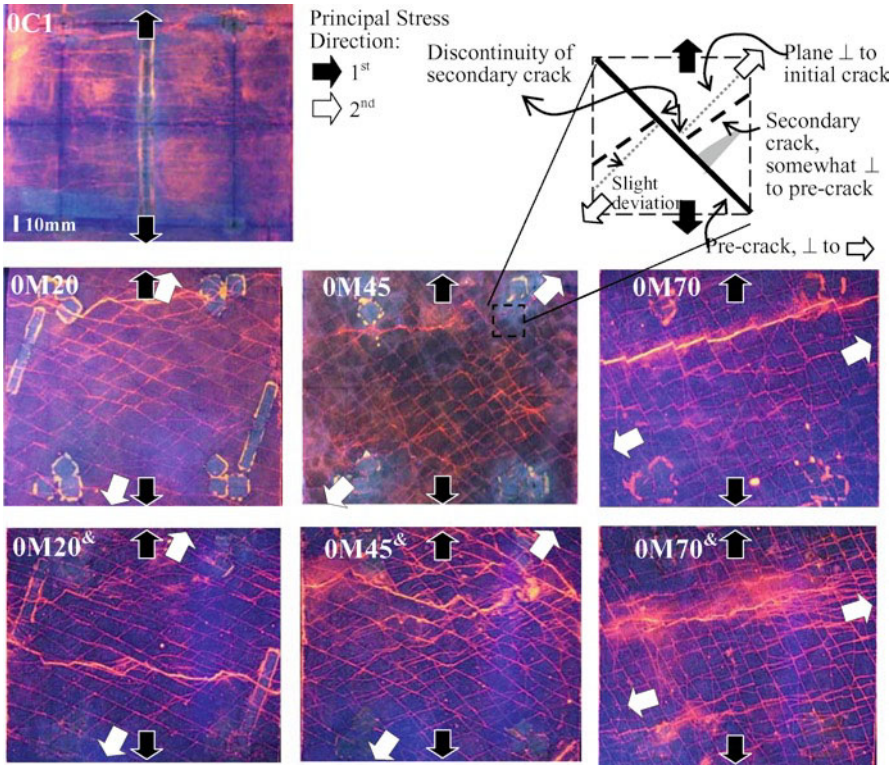

Fig. 11.8 Crack pattern of Group 0 plates after failure

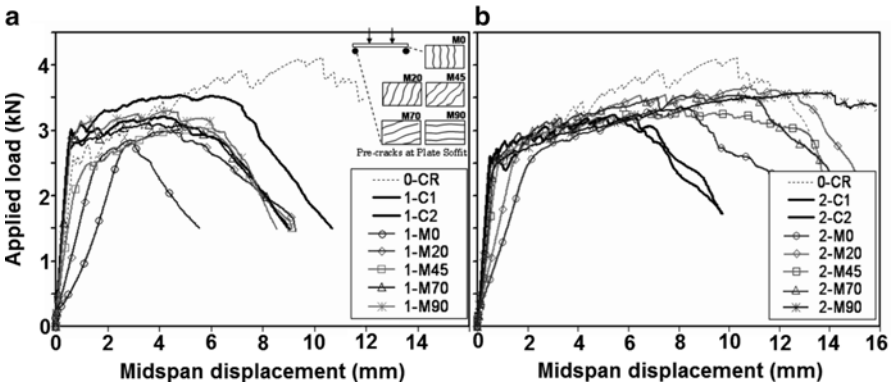

Fig. 11.9 Response of: (**a**) Group 1 plates (aggregate 30%γ_{max}) and (**b**) Group 2 (15%γ_{max})

Second, pre-cracks were uniform and continuous, while secondary cracks were discontinuous. They were uniformly spaced between 5 and 15 mm apart. Third, the pre-cracks were orthogonal to the principal stress direction of the preloading stage, while the secondary cracks always appeared near the orthogonal to the pre-cracks, with variations of up to 15°. No secondary cracks were formed orthogonal to the principal stress direction applied during the final loading stage. It should be noted that the orientation of the secondary cracks, in fact, indicates the in-plane stress-carrying mechanism of cracked ECC. The orthogonal pattern of the pre- and secondary cracks implies that the mechanism of stress transfer was relying more on the stresses developed parallel and orthogonal to the pre-cracks and less on the shear along the pre-cracks. Hence an orthogonal crack pattern resulted.

The load-midspan deflection responses of the pre-cracked plates of Group 1 and 2 are compared in Fig. 11.9. In Group 1 plates, only in Plate 1M0 was the response brittle due to premature failure at the pre-crack. The other plates in Group 1 showed a deflection-hardening response. Plates 1M20, 1M45 and 1M70 showed a comparable ductility in the range of about 4–6 mm. Slight reductions in flexural capacity were observed, of about 5–10%. This result suggests that the rotation of the principal stress direction had less impact on its macroscopic response. Nevertheless, flexural capacity and ductility of the plates were significantly below those of Plate 0CR [for clarity, see Fig. 11.10b]. Therefore, it could be surmised that the addition of excessive amount of coarse aggregate in ECC is ineffective.

Figure 11.11 shows the comparison of the crack pattern of the plates in Groups 0, 1, and 2. Note that the cracking pattern of Group 0 plates previously shown in Fig. 11.8 is again shown at the first row for a better comparison. The second and third rows indicate the cracking pattern of Group 1 and 2 plates with coarse aggregate amount of 30% and 15%γ_{max}, respectively. The different columns indicate various pre-crack orientations. Significant differences in secondary crack orientation can be observed. In all cases, the secondary cracks in Group 0 plates showed the largest deviation angle θ with respect to the plane normal to the new principal stress direction. Interestingly, θ appears to be the most acute for Group 2 plates, indicating

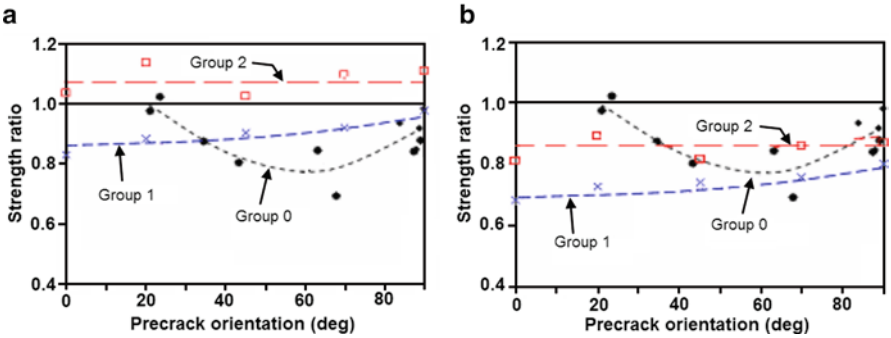

Fig. 11.10 Normalized strength based on: (**a**) the companion control plates and (**b**) Plate 0CR

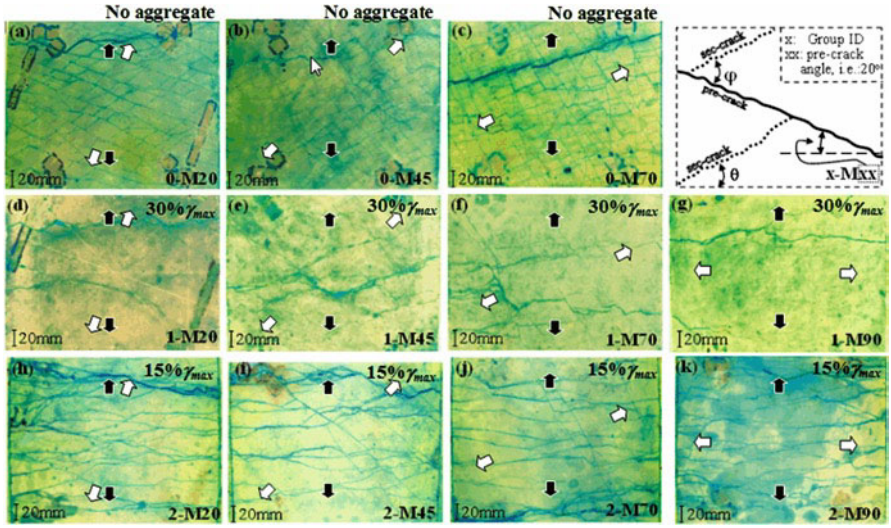

Fig. 11.11 Comparison of crack pattern among the plates with and without coarse aggregates

a better stress transfer along the pre-cracks than the other two groups. The indication is that, although the amount of coarse aggregate in Group 2 was less than that used in Group 1, the stresses across the cracks were transmitted more effectively. This might be attributed to the interaction between fiber bridging and aggregate: while the fibers confined the pre-cracks from reopening, the aggregate transmitted the occurring shear stress and limited the crack slip. The trade-off between the two should be optimized and addressed in further research.

Further observations of the cracking pattern of each plate shown in Fig. 11.11 also show that the number of secondary cracks in each plate of Group 0 and 1 is comparable to that of the corresponding control plates shown previously in Fig. 11.5. In Group 2 plates, the crack number tends to increase slightly. The increase might

be benefitted from internal microcracking that formed around the aggregate during the pre-cracking stage.

Another potentially interesting observation is that the orientations of secondary cracks θ tend to vary even in one plate, something that particularly appeared in Group 2 plates. In Plate 2 M45, for example, θ tends to increase in regions where the crack spacing is larger. This implies that the orthogonal crack pattern observed was not merely attributed to the stresses occurring at cracks, but also to the area of the uncracked parts. Further research in this area should address the effectiveness of coarse aggregate when it is used in ECC with smaller crack spacing than the one investigated herein.

11.4 Summary and Conclusions

Results from bending tests on pre-cracked ECC plates with and without the addition of coarse aggregate, subjected to principal stress rotation, are presented. From the results presented, the following conclusions can be drawn:

1. Tests on pre-cracked ECC plates subjected to principal stress rotation enable a more thorough investigation of post-cracking behavior of ECC subjected to complex stress states, involving tensile stress and shear stress transfer across multiple cracks.
2. Reorientation of the principal stress direction was found to have a significant effect on the response of cracked ECC. As the angle between the principal stress direction and the orientation of pre-existing cracks becomes larger (up to 70°), the strength apparently decreases up to about 30%. Initial stiffness appears to consistently increase with increasing angle between principal tensile stress and pre-cracks orientation.
3. When subjected to a stress rotation, ECC exhibited a nearly orthogonal crack pattern. The orthogonal pattern implies that the mechanism of stress transfer was relying more on the stresses parallel and orthogonal to the pre-existing cracks and less on interface shear transfer.
4. The addition of coarse aggregate demonstrates significant reductions in flexural capacity and flexural ductility when the applied stress direction does not rotate. In a situation when principal stress direction rotates, the test results show that the addition of aggregate can improve the performance of cracked ECC.
5. The viability to improve the performance of cracked ECC is achieved by the addition of coarse aggregate of $15\%\gamma_{max}$. The improvement is judged by the orientation of secondary cracks that became less dependent on the orientation of the pre-existing cracks, comparable flexural capacity irrespective of the reorientation of the stress fields, and ductile response. It is surmised that the addition of coarse aggregate in ECC helps the fibers in transmitting shear stress across cracks, provided that the fibers still hold the cracks from further opening.
6. The addition of an excessive amount of coarse aggregate (e.g. larger than $30\%\gamma_{max}$) is ineffective, possibly due to the significant reduction of fiber bridging at a crack and the considerable increase in the ECC matrix toughness.

References

JSCE (2007) Recommendations for design and construction of High Performance Fiber-Reinforced Cement Composite with multiple fine cracks (HPFRCC). Concrete Libr 127:129–135 (in Japanese)

Kunieda M, Rokugo K (2006) Recent progress on HPFRCC in Japan – required performance and applications. J Adv Concrete Technol 4(1):19–33

Li VC (2003) On Engineered Cementitious Composites (ECC). J Adva Concrete Technol 1(3): 215–230

Li VC, Wu HC (1992) Conditions for pseudo strain-hardening in fiber reinforced brittle matrix composites. J Appl Mech Rev 45(8):390–398

Li VC, Wang S, Wu C (2001) Tensile strain-hardening behavior of PVA-ECC. ACI Mater J 98(6): 483–492

Li VC, Lepech M, Li M (2005) Field demonstration of durable link slabs for jointless bridge decks based on strain-hardening cementitious composites. Michigan Department of Transportation Research Report no. RC-1471, p 110

Maekawa K (1983) Flow rule and plane stress constitutive equations of concrete. Concrete Eng 21(8):103–121 (in Japanese)

Naaman AE, Reinhardt HW (1996) Characterization of High Performance Fiber Reinforced Cement Composites – HPFRCC. High Performance Fiber Reinforced Cement Composites 2 (HPFRCC 2), In: Naaman AE, Reinhardt HW (eds) Proceedings of the second international RILEM workshop, E&FN Spon, London, pp 1–24

Suryanto B (2009) Mechanics of high-performance fiber-reinforced cementitious composite under principal stress rotation. PhD thesis, University of Tokyo, Japan

Suryanto B, Nagai K, Maekawa K (2010) Bidirectional multiple cracking tests on high-performance fiber-reinforced cementitious composite plates. ACI Mater J 107(5):450–460

Van Mier JGM (1985) Influence of damage orientation distribution on the multiaxial stress strain behavior of concrete. Cement Concrete Res 15:849–862